Title

Analyzing refractive index profiles of confined fluids by interferometry part II: Multilayer and asymmetric systems

Authors

Kienle, Daniel F
Kuhl, Tonya L

Publication Date

2016-09-01

DOI

10.1016/j.aca.2016.07.009

Peer reviewed

analytical chemistry

Article

pubs.acs.org/ac

Analyzing Refractive Index Profiles of Confined Fluids by Interferometry

Daniel F. Kienle and Tonya L. Kuhl*

Department of Chemical Engineering and Materials Science, University of California Davis, Davis, California 95616, United States

Supporting Information

ABSTRACT: This work describes an interferometry data analysis method for determining the optical thickness of thin films or any variation in the refractive index of a fluid or film near a surface. In particular, the method described is applied to the analysis of interferometry data taken with a surface force apparatus (SFA). The technique does not require contacting or confining the fluid or film. By analyzing interferometry data taken at many intersurface separation distances out to at least 300 nm, the properties of a film can be quantitatively determined. The film can consist of material deposited on the surface, like a polymer brush, or variation in a fluid's refractive index near a surface resulting from, for example, a concentration gradient, depletion in density, or surface roughness. The method is demonstrated with aqueous polyethylenimine (PEI) adsorbed onto mica substrates, which has a large concentration and therefore refractive index gradient near the mica surface. The PEI layer thickness determined by the proposed method is consistent with the thickness measured by conventional SFA methods. Additionally, a thorough investigation of the effects of random and systematic error in SFA data analysis and modeling via simulations of interferometry is described in detail.

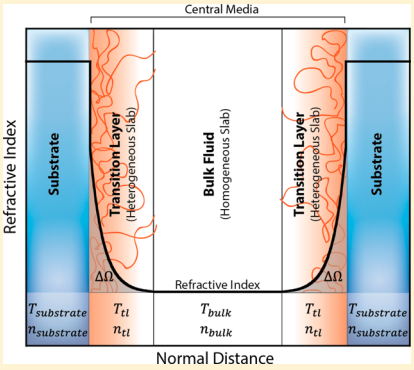

The structural properties of fluids confined between solid surfaces are valuable for interpreting fluid behavior as continuum theory breaks down. When coupled with force measurements, changes in the fluid refractive index can shed light on the mechanism of elusive surface interactions such as hydration, hydrophobic or solvation interactions. For example, such measurements could be used to determine the properties of a depletion layer near a surface like that found for water near a hydrophobic surface.[1−4] Likewise, the same approach can be applied to any adsorbed or deposited film to determine the film's thickness or refractive index and quantify the properties of any polymer, surfactant, or thin film of interest. The surface force apparatus (SFA) is an ideal instrument for this purpose because it is capable of simultaneously measuring the interaction between macroscopic surfaces and density (via refractive index) of the medium separating these surfaces. However, such measurements are challenging, due in particular to systematic error that arises from uncertainty in substrate properties and the effects of inhomogeneity in the fluid or film refractive index that is not typically accounted for in optical analysis.

Several complementary techniques are useful for measuring properties of thin films and fluids near surfaces. Ellipsometry[5] is able to give adsorbed mass but is difficult to apply to measurements in solution, which is better suited for measurement with surface plasmon resonance. Quartz crystal microbalance is capable of giving real-time estimates of the adsorbed amount, and X-ray and neutron scattering techniques[6] are capable of measuring local refractive index profiles near surfaces. However, measurement in confinement is not straightforward and has only rarely been accomplished with X-ray and neutron reflectivity.[7−12] While the SFA cannot measure the local refractive index at specific distances from the surface, the mean refractive index can be measured throughout confinement, which can elucidate the effects of confinement.

The SFA has previously been used for refractive index profile measurements (measurements taken at many separation distances) of confined polymer solutions,[13] water,[14−16] and hydrocarbons.[17,18] Kekicheff and Spalla[14] demonstrated how uncertainty in the substrate contact measurements can cause systematic error in the refractive index that is indistinguishable from true variation of the refractive index. These results call into question the accuracy of other refractive index profile measurements. The extended SFA takes advantage of advances in technology to more precisely determine the mica substrate properties, and the reduction of random error by use of this SFA setup has been demonstrated.[19] However, errors in substrate properties can have many other potential sources including particle contamination[17,20,21] and adsorbed contaminants,[17,22−27] which will have the same effects on the refractive index measurements as that described by Kekicheff and Spalla.[14] In a later paper, Heuberger and Zach[17] demonstrated how contradictory refractive index profile results can be acquired for surfaces with and without particle contamination.

Received: September 15, 2014
Accepted: November 3, 2014
Published: November 3, 2014

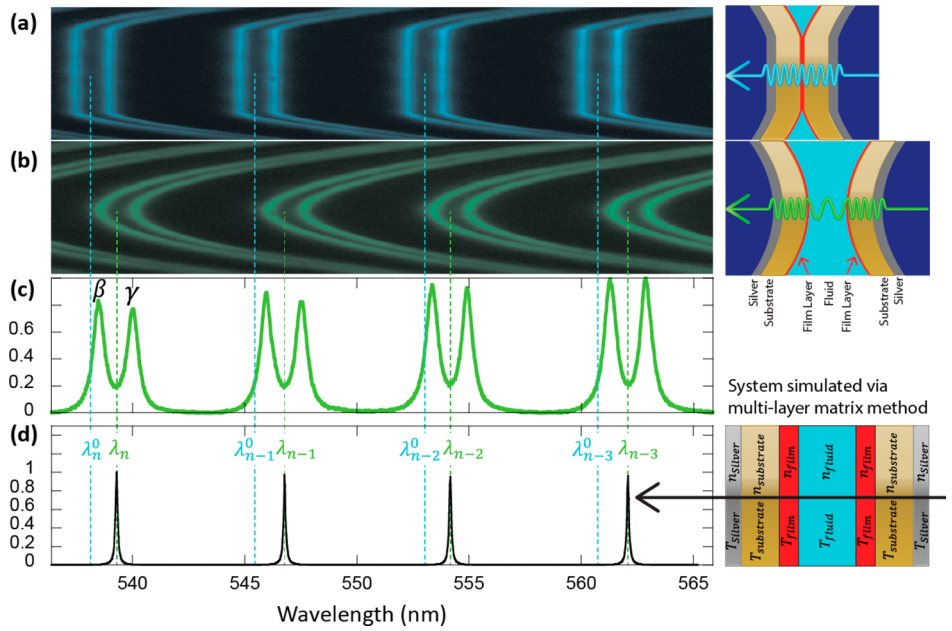

Figure 1. Examples of spectral images with surfaces (a) in compressed contact and (b) with surfaces separated. (c) Spectrum of the separated image used for analysis and (d) best-fit theoretical spectrum, where green dashed lines indicate the midpoint of the experimental β- and γ-peak wavelengths used to define the experimental fringe position to which the theoretical fringes were fit. To the right of panels a and b are illustrations of the interferometer, and to the right of panel c is a schematic of the system used to simulate the theoretical spectrum.

This work describes an algorithm for determining solvent, adsorbed layer, and/or substrate properties without contact measurements. This is useful for several systems of interest where the surfaces are fragile and could be damaged or changed by contacting them. For example, hydrophobic monolayers in water can be torn apart upon separation, and unstable bilayers are susceptible to fusion.[28,29] It is also useful for systems where changes such as plastic deformation or permanent chemical reaction may take place upon contact. Furthermore, the method could potentially be used to ascertain the roughness or lateral heterogeneity of surfaces or films. The technique works by eliminating the effects of systematic error caused by inconsistencies between contacted measurements and refractive index profile measurements. We demonstrate the technique theoretically, using realistic simulations with added random and systematic error typical of SFA experiments, and physically with experiments on an aqueous solution of cationic polyethylenimine (PEI) adsorbed onto mica substrates as a model of a medium with variations in the refractive index.

EXPERIMENTAL SECTION

Linear PEI hydrochloride salt with a molecular weight of 20k and a polydispersity index (PDI) of 1.2 was purchased from Sigma–Aldrich and stored at 4 °C. The polymer was dissolved in water to form a 100 ppm solution by weight. The water used throughout these experiments was purified with a Milli-Q gradient water purification system with a resistivity of 18 MΩ·cm.

The SFA substrates consist of back-silvered, thin mica sheets of uniform thickness. The mica was cleaved and cut by the procedure described by Israelachvili et al.[24] The mica substrates were glued silver-side-down onto two cylindrical glass discs and mounted in the SFA opposite one another in a crossed-cylinder orientation, where they form an interferometer. A droplet of PEI solution was applied between the surfaces and left for several hours. Then the SFA box (350 mL) was filled with 0.5 mM $NaNO_3$ solution and left overnight. Under these conditions, the PEI surface coverage should be laterally homogeneous.[30] To take measurements, white light from a tungsten halogen source is collimated and shone through the assembled interferometer (Figure 1), which transmits whole-order wavelengths called fringes of equal chromatic order (FECO).[31] The light is then directed into a spectrometer so the peak wavelengths can be measured and used to analyze the properties of the system.

All data analysis was done by use of software written in house that determines layer properties numerically. The measured fringe wavelengths are fit to theoretical (simulated) fringe wavelengths by varying up to two properties of the system (in this case, thickness and refractive index of the central film) to minimize the sum-squared error between the measured peak wavelengths and theoretical peak wavelengths. The theoretical spectra are generated by the multilayer matrix method,[32,33] which uses optical transfer matrices to describe the propagation of electromagnetic waves in each layer of a stratified medium. This method is derived from the Maxwell equations and is very flexible with regard to the properties of the system. Mica is birefringent, which causes each FECO to appear as a doublet with a β-peak and γ-peak. To reduce the number of computations, we used the midpoint of the fitted β- and γ-peak wavelengths as the measured peak wavelength. The experimental setup and data analysis for SFA measurement have been described in greater detail previously.[34]

Spectra were measured in flattened contact before and after addition of the polymer solution to determine the substrate and compressed polymer properties. For each profile, measurements were taken from beyond 4000 Å separation to flattened contact. The measurements taken for the experiments had up to 9 β–γ fringe doublets. Only fringes that remained in the spectrum at all separation distances were used in the analysis (typically 6–7 fringe pairs). The spectral data for noncontact measurements represent the lateral average of several square

dx.doi.org/10.1021/ac503469x | Anal. Chem. 2014, 86, 11860–11867

micrometers surrounding the point of closest approach between the curved surfaces and are taken with exposure times of several seconds. An example spectrum from separated surfaces is shown in Figure 1b. Measurements on surfaces in flattened contact (Figure 1a) are averaged over a larger area to increase the signal-to-noise ratio. We were careful to ensure that neither the optics nor the orientation of the surfaces was altered between the contact and noncontact measurements, because even slight changes in either can cause significant changes in the apparent properties of the substrate.[34]

■ ERROR SOURCES AND CORRECTIONS

Before describing the algorithm in detail, we first address sources of random and systematic error and their corrections in order to obtain quantitative measurements of the surface film or confined material properties from interferometer spectra.

Random Error in Surface Force Apparatus. The random error in the fringe wavelength can be determined from the measured spectra (Figure 1).[34] Using a Monte Carlo-type error analysis, we have determined what effect random error in the fringe wavelengths (Gaussian noise of 0.03 Å standard deviation) has on the refractive index and thickness when analyzed simultaneously at different separation distances, each with 500 iterations. The results shown in Figure 2 reveal a

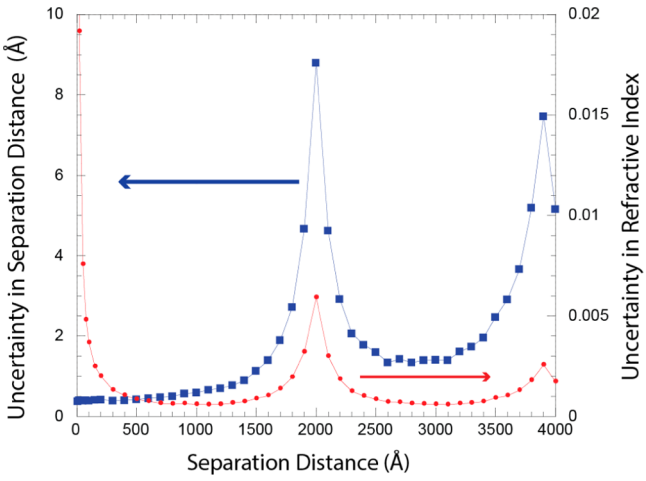

Figure 2. Theoretical uncertainty of separation distance (blue squares) and refractive index (red circles) as a result of random error on the substrate contact and profile fringe measurements, determined by simulating and analyzing fringe data, with Gaussian error added iteratively, and taking the standard deviation of the results.

periodic pattern in error sensitivity of both the thickness and refractive index, with enhanced sensitivity at separations distances of 0 and around even multiple of 1000 Å and reduced sensitivity around odd multiples of 1000 Å. This 2000 Å period in wavelength corresponds to the average interfringe distance of the contact spectrum.

Systematic Error. The most important and identifiable systematic errors in the SFA are inaccuracy in substrate properties, and inconsistencies or changes in the properties of the central film between the substrates that are unaccounted for. The latter can be caused by adsorption or removal of materials localized at the substrate between contacted and separated measurements or by variation in the fluid refractive index that exists at the substrate surface when separated but is displaced or changed when in contact. These systematic errors can be broken into three categories that exhibit different functionality. The first type results from using incorrect values for the substrate properties that are still an acceptable solution to an accurate substrate contact spectrum. This type of error arises from simultaneously varying thickness and refractive index of the substrate when analyzing the substrate contact spectrum, or fixing the refractive index of the substrate at an incorrect value, and it results in a constant offset in the refractive index of the intervening material and a proportional offset in the separation distance, such that $\Omega_{error} \approx \Omega_{actual}$ where Ω is the optical thickness of the fluid. This will be referred to as type 1 error and is shown in Figure 3a (thick blue dashed line), where an incorrect value of the refractive index of mica was used, resulting in a constant shift of 0.007 above the true optical thickness (solid black line).

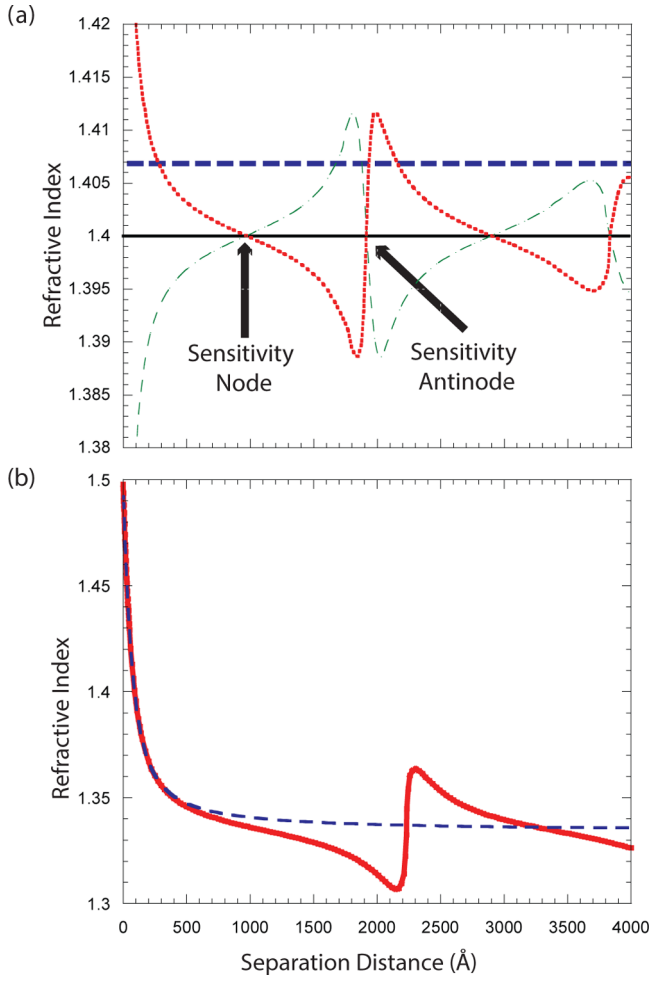

Figure 3. (a) Systematic error in refractive index profile caused by incorrect substrate thickness or refractive index with the correct optical thickness (type 1 error; thick blue dashed line) and caused by error in thickness above (type 2 error; thin green dashed line) and below (type 2 error; red dotted line) the true optical thickness (solid black line). Data were generated by simulating fringes and analyzing them with mica properties fixed at incorrect values. (b) Type 3 systematic error resulting from analyzing variable refractive index fluid with the mean refractive index at each separation distance (solid red line) along with the actual mean refractive index of the fluid (blue dashed line). Data were generated by the simulation method described in the Simulation Methods and Results section.

dx.doi.org/10.1021/ac503469x | Anal. Chem. 2014, 86, 11860−11867

The second type of error (type 2 error) results from using inaccurate or inappropriate contact fringe wavelengths (resulting from of contamination or unaccounted-for shifts in the optical path due to alterations in the optics or orientation of the substrates) to determine the properties of the substrate. This error results in a periodic trend in the refractive index with a period of around 2000 Å, similar to the random error (Figure 2), with an erroneous variation in the mean refractive index at low separation distances. This is shown in Figure 3a, where the red dotted line is the result of underestimating the substrate thickness and the thin green dashed line is a result of overestimating the substrate thickness. As expected, the refractive index converges to the true value at the separation distances with low error sensitivity (from here on referred to as sensitivity nodes) and diverges at the separations distances with high error sensitivity (from here on referred to as sensitivity antinodes). This is problematic for refractive index measurement because data at distances below the sensitivity nodes will appear to be converging toward a bulk value and variations in the refractive index are difficult to distinguish from type 2 systematic error. Unfortunately, no previous refractive index profile measurements extend beyond the sensitivity node,[13,14,17,18] so the resulting divergence has not been observed. If type 2 error is present in the analysis, type 1 error will also be present unless the substrate refractive index is accurate, in which case the sensitivity nodes will reflect the bulk refractive index of the fluid.

Type 2 error has been addressed in part by Kekicheff and Spalla[14] for water confined between hydrophobic surfaces and was attributed to uncertainty in the substrate measurement. While technological and analytical advances have reduced this uncertainty from their error of ±1 Å wavelength (which was even large at the time) to less than ±0.03 Å depending on the system specifics, we believe that the inaccuracies leading to this type of error are not purely a result of random uncertainty in substrate measurement being propagated in the analysis of subsequent layers, as suggested, but are in fact primarily systematic. This type of error may be caused by contamination such as particles[20,21] or adsorbed molecules[23−25,27,35,36] on the surface during contact or by any other inconsistencies between the substrate contact measurement and separated profile measurements, such as changes in the optics. Furthermore, it is known that there is a layer of ions on mica surfaces after cleaving that can be removed by rinsing.[16] It is also known that mica surfaces in water are hydrated even when in adhesive contact.[37] It also requires considerable pressure to displace solvent[38,39] or electrolytes[40] from between confining surfaces, which could compress and alter the apparent properties of the substrate if achieved. Thus, in many common experimental scenarios, there is a possibility that measurement of substrate properties will include adsorbed layers, even when the surfaces are free of contamination. This is generally unimportant for distance and force measurements, due to the small thickness of the adsorbed layers in most systems, but can have an observable impact on refractive index measurements throughout the entire profile if not avoided or accounted for.

Type 3 error results from treating a fluid with a continuously varying refractive index as a homogeneous film of identical thickness, with the refractive index equal to the mean value within the fluid, or ignoring adsorbed films (polymers, surfactants etc.) on the substrate during analysis. This approximation is convenient for use of matrix methods that dramatically simplify the analysis of layered optics and is used for refractive index measurements in the SFA, but it ignores reflections from within the film due to refractive index gradients, which can significantly impact the refractive index values even if the gradients are not extreme.[41] Regardless, if the substrate measurements are accurate, simulations indicate that the mean refractive index profile is within ±0.001 out to separation distances of 400 Å (disregarding random error) as shown in Figure 3b, which is typically the range of interest for SFA experiments. However, the oscillations from type 2 error are still present as a result of assuming the refractive index is constant, as can be seen at larger separations in Figure 3b. In other words, variation in the mean refractive index at small separation distances is not the result of systematic error, but the periodic trend at larger separations is. The profile is indistinguishable from type 2 error at separation distances greater than where the refractive index variations at either surface overlap (henceforth referred to as the overlap separation distance). If the surfaces reach contact at zero separation distance, then it is reasonable to conclude that the refractive index variation is not a result of substrate error and that there is no type 2 error. On the other hand, if they contact at a positive separation distance, there is no way to deconvolute type 2 and type 3 error, due to the possibility of adsorbed materials. The analytical method described in this paper focuses on correcting type 1 and type 3 errors while assuming that type 2 error is negligible, which is appropriate for clean, carefully prepared mica substrates.[24]

Algorithm for Correction of Systematic Error. The analytical method presented here uses data at many separation distances throughout the profile to add the constraint that the local refractive index is constant away from the surface. In other words, measurements must be made beyond the overlap separation distance. This allows three properties to be determined, one that is constant throughout the profile and two that vary at each separation distance. In addition to these three variables, the specific substrate properties can be determined, as long as they are still a solution to an accurate substrate contact measurement. [Note that a substrate contact measurement alone can only be used to determine either the substrate thickness or refractive index, while the other is fixed at an assumed value or measured by another method.] Finally, this can all be done without taking measurements below 1000 Å (except the substrate contact), which is useful for determining properties of films that may be damaged or altered when put into contact.

The method used to correct systematic error takes advantage of the fact that perturbation of the refractive index beyond the sensitivity node is not influenced by variations that occur upon confinement. Thus, we can find substrate and deposited layer properties where the refractive index is constant at a known bulk value. If there are inherent variations in the fluid refractive index near the substrate or there is a film on the substrate, a hypothetical "transition layer" (tl) with appropriate properties can be added between the substrate and solvent to counteract the inherent variation. This method is appropriate because an inhomogeneous or stratified film is optically equivalent to two homogeneous films.[41] The transition layer redefines the plane of contact, and the thickness and refractive index must have equal change in optical thickness from a system with constant refractive index (and no transition layer) as the actual system with varying refractive index does, satisfying eq 1, where $\Delta\Omega$ is the change in optical thickness, T_{tl} is the thickness of the transition layer, n_{tl} is the refractive index of the transition layer,

dx.doi.org/10.1021/ac503469x | Anal. Chem. 2014, 86, 11860−11867

n_{bulk} is the bulk refractive index, n_{local} is the local refractive index, and z is the normal distance from the surface. The change in the optical thickness is analogous to the areal change in mass from bulk.

$$\Delta\Omega = T_{tl}(n_{tl} - n_{bulk}) \approx \int_0^\infty [n_{local}(z) - n_{bulk}]\, dz \quad (1)$$

The refractive index profile found by incorporating the transition layer does not have a direct physical meaning because the transition layer effectively cancels any refractive index variations, leaving a central film with a constant, bulk refractive index. However, because the thickness of the actual refractive variation may not match the thickness of the transition layer, there will be a compensatory deviation from bulk refractive index at separations below the overlap separation distance. As a result, the onset of this deviation corresponds directly to the distance from the surfaces over which the true variation in the refractive index extends. If the mass of the heterogeneous region is conserved during confinement, as is expected for deposited or compressible films, there will be no deviation. The actual mean refractive index profile (n_{act}) can then be calculated by use of eq 2, where n_{fit} is the refractive index profile fit with the transition layer and D is the separation distance between the transition layers.

$$n_{act} = \frac{Dn_{fit} + 2T_{tl}n_{tl}}{D + 2T_{tl}} \quad (2)$$

The algorithm works in two main steps. The first step is to determine the specific substrate properties. This makes use of the sensitivity nodes, which should equal the known bulk refractive index of the solvent regardless of any type 2 or type 3 error. To do this, the substrate refractive index is varied and the substrate contact measurement is reanalyzed to return thickness and dispersion of the substrate at each iteration. Then the sensitivity nodes are found, and the difference between the node refractive indices and the bulk fluid refractive index is minimized according to the fitting argument in eq 3, where $n_{node,i}$ is the refractive index at the ith sensitivity node. Although only one sensitivity node is needed for this step, results will be less susceptible to random error if more are used.

$$\text{arg} = \sum (n_{node,i} - n_{bulk})^2 \quad (3)$$

The sensitivity nodes can be approximately found by determining the separation distance at which the fringes most closely bisect two contact fringes, which is accomplished by minimizing the argument described by eq 4 where λ_n is the wavelength of the nth fringe and λ_n^0 is the wavelength of the nth contact fringe.

$$\text{arg} = \sum \left| \lambda_n - \frac{\lambda_{n-1}^0 + \lambda_n^0}{2} \right| \quad (4)$$

Alternatively, the sensitivity nodes occur where the difference between the odd−even interfringe distance and the even−odd interfringe distance is maximized. This is useful for experiments where contact fringes cannot be acquired, and the sensitivity nodes can be found by maximizing the fitting argument described by eq 5. An accurate estimate of the node distance can be found by fitting the argument described by eq 5 within a few hundred angstroms separation distance of each node to a quadratic equation and finding the maximum.

$$\text{arg} = \sum |2\lambda_n - \lambda_{n-1} - \lambda_{n+1}| \quad (5)$$

The second step of the analysis determines the optical thickness of the transition layer by minimizing the standard deviation of the fluid refractive index around the sensitivity antinode. This is done systematically by using data between the first and second sensitivity nodes. At the solution, the divergence of the refractive index at the sensitivity antinodes is eliminated and any type 3 error is corrected. The specific refractive index and thickness of the transition layer cannot be found independently. Instead, the transition layer refractive index is fixed at an estimate, and the thickness is varied. Solutions are best found with a direct search algorithm when this method is used. In reality, the resulting $\Delta\Omega$ has a weak linear dependence on the estimate of the refractive index of the transition layer. In systems we have measured and simulated, the deviation in $\Delta\Omega$ resulting from fixing the transition layer refractive index at an inaccurate value is below the uncertainty in our results for a large range of transition layer refractive indices (± 0.25). However, considering that the dependency will be different between differing systems, it is important to verify that the effect of this dependency is not significant, particularly for experiments where the transition layer refractive index cannot be estimated within a narrow range. This can be done simply by running the second step of the analysis with the transition layer refractive index fixed at different values. Our simulations indicate that the deviation of $\Delta\Omega$ is roughly equal in magnitude to the inaccuracy of the refractive index estimate, while the sign of the deviation depends on the sign of $\Delta\Omega$.

A schematic of the full algorithm and an illustration and description of the results are shown in Supporting Information. At this point the full profile of refractive index data is reanalyzed with the corrected substrate refractive index and added transition layer, and the full mean refractive index profile can be calculated by use of eq 2.

SIMULATION METHODS AND RESULTS

The correction method was first tested by using realistic, simulated data based on an aqueous system with an adsorbed layer of PEI on the mica substrates. The error-free refractive index profile fringes and substrate contact fringes were generated by the multilayer-matrix method from specified interferometer properties. Data were generated for a system with a variable refractive index describe by eq 6 where z is the distance from the substrate:

$$n_{local} = (1.5 - 1.334)e^{-z/20} \quad (6)$$

This exponentially decaying refractive index profile was chosen as a simple model for the adsorbed PEI layer in water, where the bulk refractive index of PEI is set to 1.5.

The inclusion of a variable refractive index film away from the substrate can be modeled with a power series to approximate the nonanalytical expression for the electric field that arises from including normal variations in the refractive index. With this approximation, the characteristic matrix of a nonhomogeneous dielectric film with normal incidence can be defined by eqs 7−9 with a second-order expansion. Here k is the wavenumber, n is the refractive index, z is the distance normal to the surface, d is the thickness of the layer, Z_0 is the impedance of free space, and $\mathbf{M}$ is the transfer matrix for use in the multilayer matrix method.[32] A detailed derivation of these

equations and higher-order expansions are described by Jacobsson (section 3.1).[41]

$$\mathbf{M}_{\text{heterogeneous}} = \begin{bmatrix} 1 - k^2 \int_0^d n^2 \mathcal{B}\, dz & -ik\mathcal{B} \\ -ik\mathcal{A} & 1 - k^2 \int_0^d n^2 \mathcal{A}\, dz \end{bmatrix} \quad (7)$$

$$\mathcal{A} = \frac{1}{Z_0} \int_0^z n^2\, dz \quad (8)$$

$$\mathcal{B} = Z_0 z \quad (9)$$

This method is accurate for thin films with low-order expansions[41] in k. In the case of a fluid between two surfaces with inherent refractive index variation near the surfaces, the fluid layer can be broken into three layers: a homogeneous film at the bulk refractive index sandwiched between two heterogeneous films, as shown in Figure 4. This keeps the

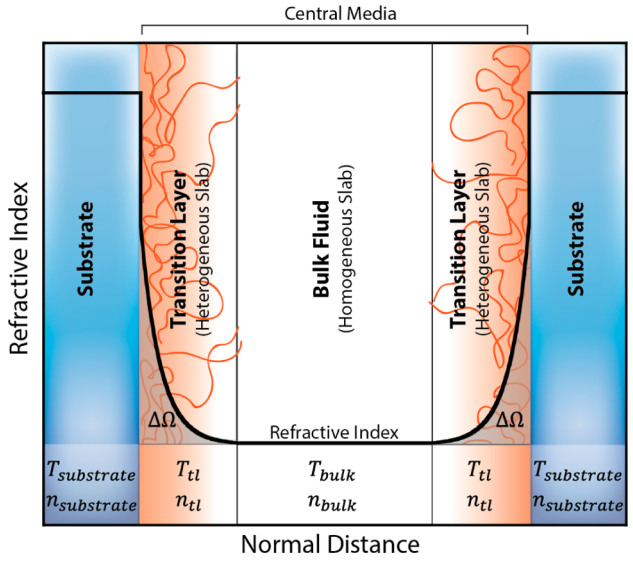

Figure 4. Plot of the local fluid refractive index with normal position through a model sample. Each slab would be represented by a different characteristic matrix to be used in multilayer matrix method analysis.

length scale of the heterogeneous films small, allowing for accurate solutions with a low-order expansion, even at large separation distances. It is important to note that the heterogeneous films at either surface cannot be treated as identical and thus the system has to be analyzed as an asymmetric interferometer. For systems where the heterogeneous film extends far into the fluid, higher-order expansions are required. Further expansion is tedious but straightforward.[41] A simple way to check whether a higher-order expansion is necessary is to simulate fringes by use of the equations above and compare them to a system where the fluid is modeled by a large number of thin homogeneous layers. This is a simple but computationally expensive extension of the multilayer matrix method. A model including terms up to powers of k^4 was necessary for the simulations in this study, because the heterogeneous slabs extended far into the central fluid and substantial inaccuracies were observed when lower-order expansions were used.

With the ideal system well modeled, we next address the contribution of random and systematic error. First, Gaussian noise of standard deviation 0.03 Å (which was found to be typical for our system)[34] was added to the fringe data to simulate peak wavelength uncertainty. To add type 1 systematic error, we analyzed the substrate thickness and dispersion with the refractive index fixed at a deliberately incorrect value. Type 2 error is ignored, on the basis of the assumption that clean substrates were used. Finally, type 3 systematic error was induced by incorporating variation in the fluid refractive index due to the adsorbed polymer layer. The simulated data were analyzed with the middle layer treated as a single homogeneous layer (bulk water) by the new analytical method. Figure 5

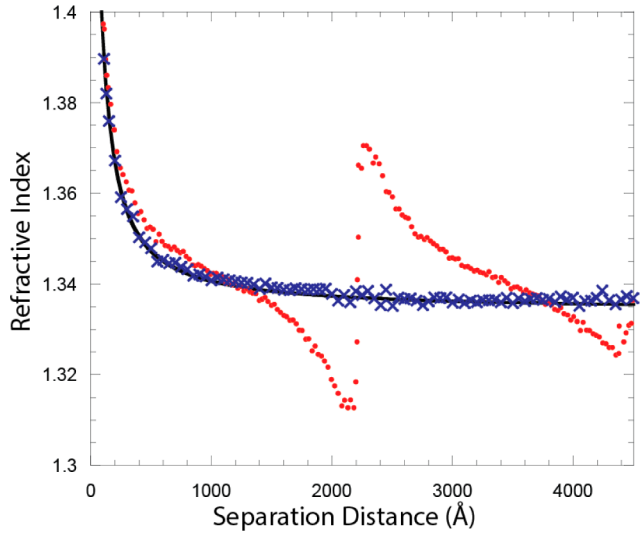

Figure 5. Plot of realistic simulated refractive index profile data of a system with an increasing refractive index at low separation distances (simulated by use of eq 7), analyzed with a constant refractive index at each separation distance (red circles) and with a mean refractive index found after determining substrate and transition layer properties by the methods described (blue ×). Actual mean refractive index is shown by the solid line.

shows the mean refractive index profile before (red circles) and after (blue ×) the simulated data (simulated by use of eqs 7–9 and the three-slab method) were analyzed with the methods described above, along with the mean refractive index used to generate the data (black line). The corrected data are well described by the error-free profile, indicating that our correction method effectively removed the systematic errors even when realistic random error was included.

The transition layer found had $\Delta\Omega$ = 3.4 ± 0.2 Å, and the $\Delta\Omega$ used for the simulation was 3.32 Å, which are in excellent agreement. At the input refractive index of 1.5, $\Delta\Omega$ corresponds to a dry film thickness of 20 ± 1 Å, which is the accuracy typically expected from SFA measurements. Thus, the analytical method is theoretically feasible. To determine the uncertainty of the transition layer $\Delta\Omega$ from the simulation, which arises as a result of random error in the fringe wavelengths, the same data were reanalyzed 100 times with new random Gaussian error added before each analysis, and the standard deviation was taken of the results.

dx.doi.org/10.1021/ac503469x | Anal. Chem. 2014, 86, 11860–11867

EXPERIMENTAL RESULTS AND DISCUSSION

As a direct demonstration of this analytical technique, we measured the optical thickness of aqueous PEI adsorbed onto mica by the method described (without contacting the adsorbed PEI surfaces), and compared this to highly compressed contact measurements of the PEI-coated surfaces. $\Delta\Omega$ of the transition layer was 1.9 ± 0.2 Å, which is the average of four experiments, and corresponds to $\Delta\Omega$ of the adsorbed polymer on each surface. The uncertainty of transition layer measurement was determined by a block bootstrap analysis, which is appropriate if the data are fine-grained enough to exhibit systematic features after resampling. The data were split into blocks of three data points, one data point from each block was randomly selected, and the set was analyzed. This was repeated 20 times for each experiment, and the uncertainty on the optical thickness of the transition layer was taken as the standard deviation. The value found was the same as the standard deviation of the optical thickness data.

The thickness and refractive index of the compressed polymer layer were 9.9 ± 0.2 Å and 1.520 ± 0.007, respectively, giving $\Delta\Omega$ = 1.84 ± 0.2 Å, which is within error of the analyzed profile measurements. The uncertainty in this measurement is determined by Monte Carlo error analysis as described by Kienle et al.[34] The high refractive index of this measurement suggests that nearly all the water was displaced from the polymer under compression, making this comparable to a dry thickness. Given the bulk value for branched PEI of 1.53, we can estimate the thickness of the compressed polymer from the transition layer $\Delta\Omega$ by use of eq 1, giving a compressed thickness of 10.5 ± 0.8 Å. This demonstrates that the mass of the polymer between the surfaces is conserved through confinement and shows that the analytical method described can achieve the accuracy expected of SFA experiments. The grafting density was calculated from the result to be 1.07 ± 0.08 mg/m^2, and the hydrodynamic thickness was found to be around 35 Å from force profile results. Therefore, the molecules have a flat conformation as expected for a polycation solution of low ionic strength on a negatively charged surface, with loops and tails extending out to 35 Å.

The refractive index profile for one example data set is shown in Figure 6. The plot demonstrates that the analysis was effective in removing type 3 error. For this particular data set, it was not necessary to correct for type 1 error. The right axis indicates the mass fraction of the polymer, which was approximated by use of eq 10 where x_{PEI} is the volume fraction of the PEI, $n_{measured}$ is the mean refractive index in the cavity, and n_{PEI} and n_{water} are the bulk refractive indices of PEI and water:

$$x_{PEI} = \frac{n_{measured} - (1 - x_{PEI})n_{water}}{n_{PEI}} \quad (10)$$

The correction still shows a small oscillation at the sensitivity antinode. The residual perturbation is within the expected uncertainty at these separation distances (see Figure 2). However, this is clearly a systematic effect that could not be eliminated by use of a transition layer (see Supporting Information for information on handling alternative sources of systematic errors). We attribute this small error to secondary fringes resulting from a mismatched refractive index of the glue layer and glass disc, which can occasionally cause low-amplitude unrelated interference with the refractive index data, depending on the thickness of the glue. The heightened sensitivity at the sensitivity antinode amplifies this glue effect, resulting in oscillations that cannot be removed with the method described.

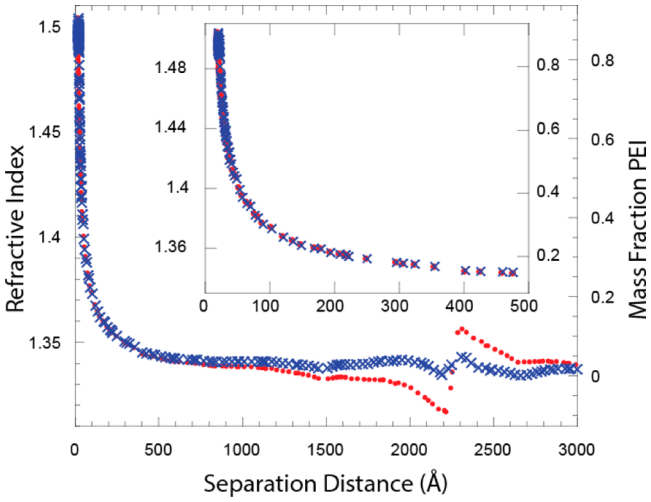

Figure 6. Plot of refractive index profile of adsorbed PEI analyzed without transition layer (red circles) and the mean refractive index profile found by use of the transition layer analysis (blue ×). (Inset) Close-up of profiles at low separation distance.

CONCLUSIONS

An analytical method that can determine specific substrate and film or heterogeneous fluid properties near a surface, without confinement of the fluid or contacting the surfaces, was described in the context of interferometric measurements as utilized in the SFA. The method works by analyzing data at multiple separation distances beyond confinement and modeling variable refractive index as multiple surface layers, which enables extraction of the film thickness and refractive index. The method was demonstrated with realistic simulated data with added error of magnitude similar to experimental error in typical SFA experiments. The analyzed simulation returned the expected values with excellent error bounds. Physical experiments on a polymer film of PEI adsorbed from water were also analyzed as a demonstration of the technique. The analysis returned a film thickness of 10.5 ± 0.8 Å with a refractive index of 1.52, which is within error of the compressed thickness measurement of 9.9 ± 0.2 Å with a refractive index of 1.520 ± 0.007. The technique provides a way of determining film properties while avoiding potentially damaging or film-altering contact. It can also be used to measure the optical thickness of depletion layers or similar films that do not exist when the surfaces are in contact. Finally, strategies to eliminate the effects of systematic and random error at various separation distances in SFA apparatus experiments were described and demonstrated in detail.

ASSOCIATED CONTENT

Supporting Information

Additional text and equations and two figures giving the algorithm, illustration, and description of the results at each step of the analysis, as well as alternative sources of systematic errors. This material is available free of charge via the Internet at http://pubs.acs.org/.

AUTHOR INFORMATION

Corresponding Author

*E-mail tlkuhl@ucdavis.edu.

Notes

The authors declare no competing financial interest.

ACKNOWLEDGMENTS

Acknowledgment is made to the Donors of the American Chemical Society Petroleum Research Fund for support of this research and to the Jeff and Diane Child/Steve Whitaker fund for Distinguished Teaching and Scholarship.

REFERENCES

(1) Poynor, A.; Hong, L.; Robinson, I. K.; Granick, S.; Zhang, Z.; Fenter, P. A. *Phys. Rev. Lett.* **2006**, *97*, No. 266101.
(2) Chattopadhyay, S.; Uysal, A.; Stripe, B.; Ha, Y. G.; Marks, T. J.; Karapetrova, E. A.; Dutta, P. *Phys. Rev. Lett.* **2010**, *105*, No. 037803.
(3) Mezger, M.; Reichert, H.; Schoder, S.; Okasinski, J.; Schroder, H.; Dosch, H.; Palms, D.; Ralston, J.; Honkimaki, V. *Proc. Natl. Acad. Sci. U.S.A.* **2006**, *103*, 18401−18404.
(4) Mezger, M.; Sedlmeier, F.; Horinek, D.; Reichert, H.; Pontoni, D.; Dosch, H. *J. Am. Chem. Soc.* **2010**, *132*, 6735−6741.
(5) Mccrackin, F. L.; Passaglia, E.; Stromberg, R. R.; Steinberg, H. L.. *J. Res. Natl. Bur. Stand., Sect. A* **1963**, *67*, 363−377.
(6) Russell, T. P. *Mater. Sci. Rep.* **1990**, *5*, 171−271.
(7) Seeck, O. H.; Kim, H.; Lee, D. R.; Shu, D.; Kaendler, I. D.; Basu, J. K.; Sinha, S. K. *Europhys. Lett.* **2002**, *60*, 376−382.
(8) Mulder, D. J.; Kuhl, T. L. *Soft Matter* **2010**, *6*, 5401−5407.
(9) Hamilton, W. A.; Smith, G. S.; Alcantar, N. A.; Majewski, J.; Toomey, R. G.; Kuhl, T. L. *J. Polym. Sci., Part B: Polym. Phys.* **2004**, *42*, 3290−3301.
(10) Kuhl, T. L.; Smith, G. S.; Israelachvili, J. N.; Majewski, J.; Hamilton, W. *Rev. Sci. Instrum.* **2001**, *72*, 1715−1720.
(11) Perret, E.; Nygard, K.; Satapathy, D. K.; Balmer, T. E.; Bunk, O.; Heuberger, M.; van der Veen, J. F. *J. Synchrotron Radiat.* **2010**, *17*, 465−472.
(12) Chodankar, S.; Perret, E.; Nygard, K.; Bunk, O.; Satapathy, D. K.; Marzal, R. M. E.; Balmer, T. E.; Heuberger, M.; van der Veen, J. F. *EPL* **2012**, *99*, No. 26001.
(13) Schmitt, F. J.; Park, C.; Simon, J.; Ringsdorf, H.; Israelachvili, J. *Langmuir* **1998**, *14*, 2838−2845.
(14) Kekicheff, P.; Spalla, O. *Langmuir* **1994**, *10*, 1584−1591.
(15) Christenson, H. K. *J. Colloid Interface Sci.* **1985**, *104*, 234−249.
(16) Kohonen, M. M.; Christenson, H. K. *Langmuir* **2000**, *16*, 7285−7288.
(17) Heuberger, M.; Zach, M. *Langmuir* **2003**, *19*, 1943−1947.
(18) Heuberger, M.; Zach, M.; Spencer, N. D. *Science* **2001**, *292*, 905−908.
(19) Heuberger, M. *Rev. Sci. Instrum.* **2001**, *72*, 1700−1707.
(20) Kohonen, M. M.; Meldrum, F. C.; Christenson, H. K. *Langmuir* **2003**, *19*, 975−976.
(21) Ohnishi, S.; Hato, M.; Tamada, K.; Christenson, H. K. *Langmuir* **1999**, *15*, 3312−3316.
(22) Frantz, P.; Salmeron, M. *Tribol. Lett.* **1998**, *5*, 151−153.
(23) Israelachvili, J. N.; Adams, G. E. *J. Chem. Soc., Faraday Trans. 1* **1978**, *74*, 975−1001.
(24) Israelachvili, J. N.; Alcantar, N. A.; Maeda, N.; Mates, T. E.; Ruths, M. *Langmuir* **2004**, *20*, 3616−3622.
(25) Raviv, U.; Klein, J. *Science* **2002**, *297*, 1540−1543.
(26) Raviv, U.; Laurat, P.; Klein, J. *Nature* **2001**, *413*, 51−54.
(27) Christenson, H. K.; Israelachvili, J. N. *J. Colloid Interface Sci.* **1987**, *117*, 576−577.
(28) Benz, M.; Gutsmann, T.; Chen, N. H.; Tadmor, R.; Israelachvili, J. *Biophys. J.* **2004**, *86*, 870−879.
(29) Helm, C. A.; Israelachvili, J. N. *Makromol. Chem., Macromol. Symp.* **1991**, *46*, 433−437.
(30) Finessi, M.; Sinha, P.; Szilagyi, I.; Popa, I.; Maroni, P.; Borkovec, M. *J. Phys. Chem. B* **2011**, *115*, 9098−9105.
(31) Israelachvili, J. N. *J. Colloid Interface Sci.* **1973**, *44*, 259−272.
(32) Born, M.; Wolf, E. *Principles of Optics*, 6th ed.; Pergamon: Oxford, U.K., 1980.
(33) Clarkson, M. T. *J. Phys. D: Appl. Phys.* **1989**, *22*, 475−482.
(34) Kienle, D. F.; de Souza, J. V.; Watkins, E. B.; Kuhl, T. L. *Anal. Bioanal. Chem.* **2014**, *406*, 4725−4733.
(35) Christenson, H. K. *J. Phys. Chem.* **1993**, *97*, 12034−12041.
(36) Ostendorf, F.; Schmitz, C.; Hirth, S.; Kuhnle, A.; Kolodziej, J. J.; Reichling, M. *Langmuir* **2009**, *25*, 10764−10767.
(37) Quirk, J. P.; Pashley, R. M. *J. Phys. Chem.* **1991**, *95*, 3300−3301.
(38) Christenson, H. K.; Gruen, D. W. R.; Horn, R. G.; Israelachvili, J. N. *J. Chem. Phys.* **1987**, *87*, 1834−1841.
(39) Horn, R. G.; Israelachvili, J. N. *J. Chem. Phys.* **1981**, *75*, 1400−1411.
(40) Pashley, R. M.; Israelachvili, J. N. *J. Colloid Interface Sci.* **1984**, *101*, 511−523.
(41) Jacobsson, R. *Prog. Opt.* **1966**, *5*, 247−286.